

Heterogeneities in granular dynamics

A. Mehta^{*†}, G. C. Barker[‡], and J. M. Luck[§]

^{*}S. N. Bose National Centre for Basic Sciences, Block JD Sector III Salt Lake, Calcutta 700 098, India; [†]The Institute of Food Research, Colney, Norwich NR4 7UA, United Kingdom; and [§]Institut de Physique Théorique, Commissariat à l'Énergie Atomique Saclay, F-91191 Gif-sur-Yvette, France

Edited by Sam Edwards, University of Cambridge, Cambridge, United Kingdom, and approved March 14, 2008 (received for review December 13, 2007)

The absence of Brownian motion in granular media is a source of much complexity, including the prevalence of heterogeneity, whether static or dynamic, within a given system. Such strong heterogeneities can exist as a function of depth in a box of grains; this is the system we study here. First, we present results from three-dimensional, cooperative and stochastic Monte Carlo shaking simulations of spheres on heterogeneous density fluctuations. Next, we juxtapose these with results obtained from a theoretical model of a column of grains under gravity; frustration via competing local fields is included in our model, whereas the effect of gravity is to slow down the dynamics of successively deeper layers. The combined conclusions suggest that the dynamics of a real granular column can be divided into different phases—ballistic, logarithmic, activated, and glassy—as a function of depth. The nature of the ground states and their retrieval (under zero-temperature dynamics) is analyzed; the glassy phase shows clear evidence of its intrinsic (“crystalline”) states, which lie below a band of approximately degenerate ground states. In the other three phases, by contrast, the system jams into a state chosen randomly from this upper band of metastable states.

granular physics | heterogeneous phases | glassy dynamics | intrinsic states

Many of the most interesting properties of granular media (1–5) arise from their athermal nature, i.e., that grains are too massive to move in response to the ambient temperature; in particular, granular dynamics are strongly hysteretic and bear the imprint of configurational histories. Heterogeneity is yet another consequence of the lack of Brownian diffusion; different parts of the same system can sustain diverse structures, and have different dynamical behavior, in the absence of sufficiently strong external perturbations.

One of the earliest indications of such heterogeneity was found in the experiments of Nagel *et al.* (6) in their investigation of Edwards' compactness (7), the “slow” effective temperature of a granular medium; their findings indicated that this, along with average density, varied strongly throughout the system. For an interesting generalization of this idea, see also ref. 8. The presence of force chains (9, 10) is another strong indicator of heterogeneity; it has been argued recently (11) that the carriers of these force chains are granular bridges (12), which are structural heterogeneities unique to granular media.

The aspect of heterogeneity that we investigate here is most similar to that investigated experimentally in ref. 6; we examine, analytically and via computer simulations, the heterogeneities that arise as a function of depth in a system of grains, having to do with density fluctuations, as well as the retrieval of ground states. Our computer simulation algorithm (13, 14) is a stochastic and cooperative hybrid Monte Carlo scheme, which models the shaking of spheres in three dimensions via alternating periods of dilation and quench; it has long been recognized as capable of modeling much of the complexity of granular media (15), and is in quantitative agreement with molecular-dynamics simulations of frictional grains (16). Details of the simulations can be found in the supporting information (SI) *Text*.

Results of Computer Simulations

We have simulated the shaking of a box of 1,300 spheres, divided (arbitrarily) into eight horizontal slices; the shaking intensity

chosen is in the intermediate range, in that it gives an additional 40% free volume on average to every sphere in the system during the dilation phase. The box has dimensions $\approx 8 \times 8 \times 18$ sphere diameters; horizontal boundaries are periodic, the lower boundary is a hard plane and the upper surface is free. The shaking algorithm is a hybrid, including both Monte Carlo compression and event-driven stabilization phases, in the presence of strong gravity (upward moves are impossible during recompression). It is thus impossible to define a time scale for the dynamics; each cycle can, however, be considered as a reorganization of the whole system in response to a single “tap.”

The results are shown in Fig. 1 *Upper*. There are eight plots of macroscopic (space-averaged) density $\phi(t)$ against time t ; each plot corresponds to a slice arranged in order of progressive depth along the column. The data are replotted in a cumulative fashion in Fig. 1 *Lower* to show the total range over which the density fluctuations occur in the column.

Two clear features emerge; the first of these is that the time-averaged value of ϕ , about which temporal fluctuations occur, is an increasing function of depth. The second of these seems rather more surprising; the range of density fluctuations is greatest in the middle of the box, at least for our times of observation. A moment's reflection, however, shows that this is to be expected for intermediate shaking intensities (13, 14): Although the top is barely fluidized, with few fluctuations about an overall low density, the jammed region near the bottom also has only very slow density fluctuations (1). It is therefore in the middle that rapid fluctuations in $\phi(t)$ are most to be expected because of quickly changing particulate environments, which can range from jammed to loosely packed, as a function of time.

Another illustration of dynamical diversity can be found in the particle tracks of Fig. 2; green tracks represent the trajectory of a tracked particle (projected onto the $x-z$, $x-y$, and $y-z$ planes) with start and end points marked in red. A particle, initially picked from the middle of the box, is essentially able to traverse the whole system: its fluid-like trajectory near the top of the box is shown in Fig. 2 *Upper*. Approximately 10,000 shake cycles later, it moves to near the base of the box; Fig. 2 *Lower* shows that its ensuing trajectory is jammed (17, 18). Note that the strong density fluctuations corresponding to the middle of the box (see Fig. 1) are uniquely responsible for the release of particles to such spatial extremes and for the subsequent manifestation of characteristically heterogeneous dynamics. We mention in passing that these tracks are qualitatively similar (19) to those observed in particle tracking experiments in dense colloidal suspensions (20), where dynamical heterogeneities were observed.

Theoretical Models

To gain a more complete understanding of the above issues, we constructed a related series of theoretical models (21–23), which

Author contributions: A.M., G.C.B., and J.M.L. designed research; A.M., G.C.B., and J.M.L. performed research; G.C.B. and J.M.L. analyzed data; and A.M. wrote the paper.

The authors declare no conflict of interest.

This article is a PNAS Direct Submission.

[†]To whom correspondence should be addressed. E-mail: anita@bose.res.in.

This article contains supporting information online at www.pnas.org/cgi/content/full/0711733105/DCSupplemental.

© 2008 by The National Academy of Sciences of the USA

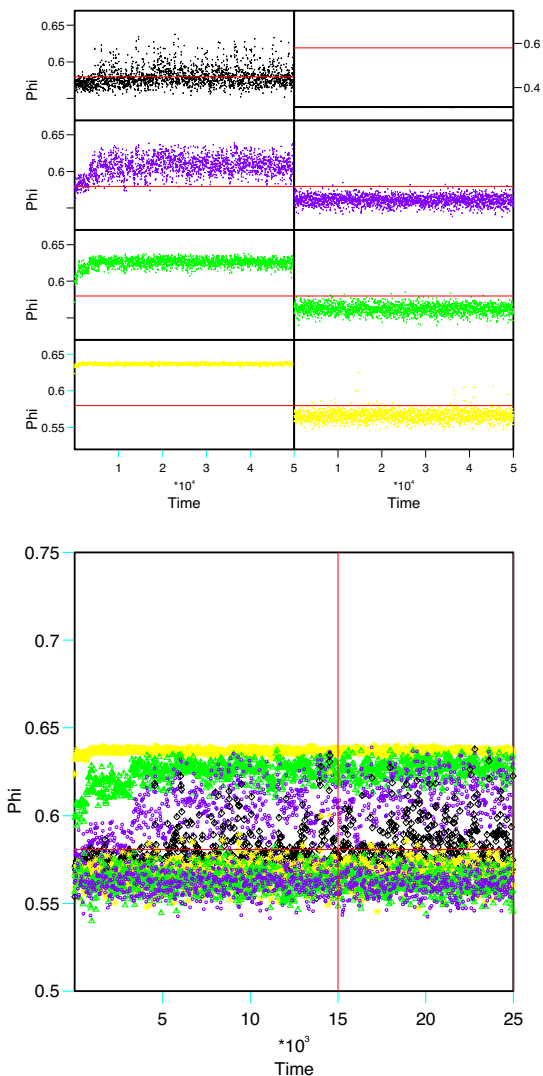


Fig. 1. Densities ϕ of successive layers of a box of grains are plotted against time. (*Upper*) The top right-hand corner represents the uppermost layer, with the three below it representing layers below itself. The traces of the next (fifth) deepest layer appear in the top left-hand corner, whereas the bottom left-hand corner represents the eighth layer nearest the base. (*Lower*) A cumulative plot of the above—the top trace in yellow represents the density of the layer nearest the base, whereas the bottom traces in black represent the top layer. Notice that the greatest fluctuations appear in the middle range of densities, corresponding to the middle of the column—an example is the purple trace corresponding to layer six.

added complexity progressively to a simple starting point. The earliest model (21) was of a shaken box of grains with translational and orientational degrees of freedom in the presence of gravity; successively deep layers were hindered in their dynamics simply because of the weight of grains above them. Heterogeneous dynamics, which ranged from fluid-like to jammed, were manifested as a function of a single parameter ζ_{dyn} , a characteristic length that determined the speed of response of a given granular layer. Long-range orientational interactions to model jamming were added to this basic model in ref. 22 via a local field h_n that measured excess void space (12) in the granular column above grain n ; each grain n was constrained to minimize its local field h_n by choosing one of two possible orientations (“disordered” or “ordered”). The disordered orientation of a grain was associated with a void of size ε ; because ε was allowed to be arbitrary, the model allowed us to differentiate between regu-

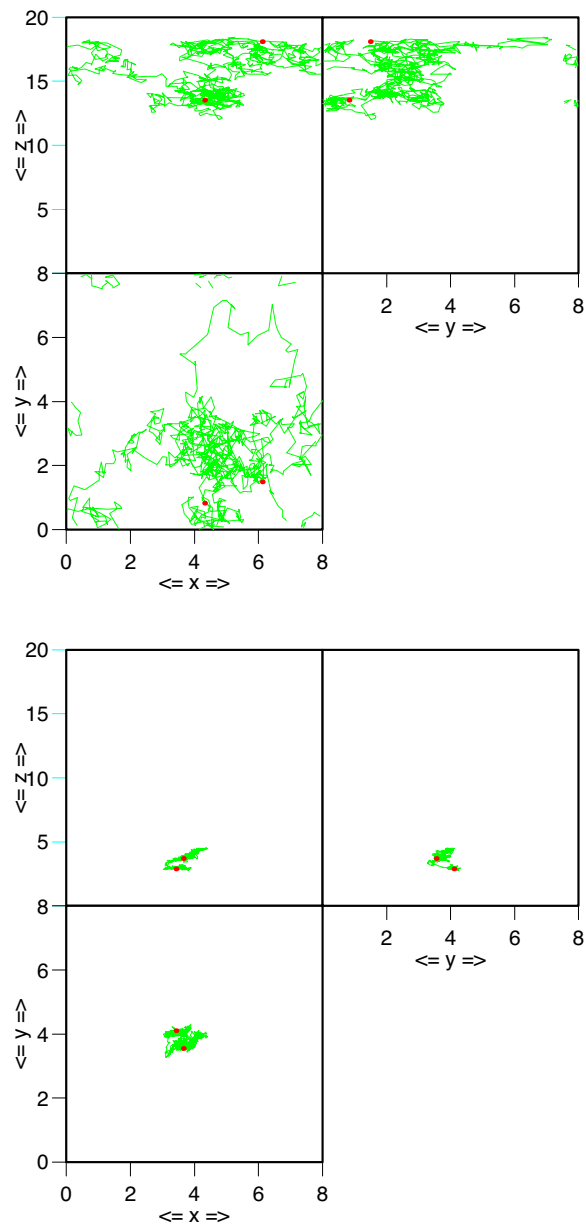


Fig. 2. Simulation results for the trajectories of a single particle (initially located in the middle of the column) in the $x-y$, $y-z$, and $x-z$ planes, as it exhibits dynamical heterogeneity via its spatial explorations. In the *Upper* figure, the particle inhabits the upper part of the box, whereas in the *Lower* figure, it has become localized in the lower regions. Each figure corresponds to $\approx 1,000$ consecutive shake cycles. The two trajectories are separated by $\approx 10,000$ shake cycles. Notice the fluid-like/free nature of the particle tracks in the *Upper* figure and their jammed appearance in the *Lower* figure, where the particle is clearly constrained by its neighbors.

larly (rational ε) and irregularly (irrational ε) shaped grains. A particularly striking prediction was that regularly shaped grains did not spontaneously retrieve their (perfectly ordered and very degenerate) ground states but, rather, gave rise to density fluctuations as a function of depth, as first indicated by the experiments of ref. 6. Another prediction was that of the anticorrelations of grain displacements [often referred to as “dynamical heterogeneities” (25)] near jamming; this was in reassuring agreement with the results of independent three-dimensional simulations of shaken sphere packings (13, 14).

In our most recent model (23), frustration (26) is added to all of the above ingredients via a local field j_n , due to the effect of

grains below grain n ; each grain is now torn between orientations suggested by the “downward” field h_n and the “upward” field j_n . The effect of j_n is expected to be strongest at the base and modulated in its upward progression by intergrain correlations; this is modeled by an exponential dependence involving a characteristic length ζ_{int} . Depths within this “frustrated” column model are consequently probed in terms of the ratios of ζ_{dyn} and ζ_{int} to the system size N , where the combination of these ratios is adequate to pinpoint a spatial region of the column (23). The model exhibits full heterogeneity in its dynamics as a function of depth: The ballistic and logarithmic phases (with their depth-dependent density fluctuations) of the earlier model (22) are retained, whereas additions include a glassy phase with slow and intermittent dynamics near the jammed (24) base.

The Frustrated Column Model: Definition and Governing Equations.

Grain orientations $\sigma_m = \pm 1$ in the frustrated model (18) are updated with the rates

$$\begin{cases} w(\sigma_n = +1 \rightarrow \sigma_n = -1) = \exp\left(-\frac{\lambda_n + H_n}{\Gamma}\right), \\ w(\sigma_n = -1 \rightarrow \sigma_n = +1) = \exp\left(-\frac{\lambda_n - H_n}{\Gamma}\right), \end{cases} \quad [1]$$

where Γ is a dimensionless vibration intensity, and λ_n is an activation energy felt by grain n , which increases linearly with the depth n , so that the local frequency

$$\omega_n = \exp\left(-\frac{\lambda_n}{\Gamma}\right) = \exp\left(-\frac{n}{\zeta_{\text{dyn}}}\right) \quad [2]$$

falls off exponentially, with a characteristic length ζ_{dyn} . This dynamical length corresponds to the depth of the boundary layer beyond which grains are frozen out by the sheer weight of grains above them. H_n is the local ordering field, which is a net measure of excess void space (12) felt by grain n due to all of the other grains; this is determined by grains both above and below itself, through constituent fields h_n and j_n , respectively:

$$H_n = h_n + g j_n, \quad [3]$$

with the coupling constant g typically assumed to be small. More explicitly, h_n and j_n are given by

$$h_n = \sum_{m=1}^{n-1} f(\sigma_m), \quad [4]$$

$$j_n = \sum_{m=n+1}^N f(\sigma_m) \exp\left(-\frac{m-n}{\zeta_{\text{int}}}\right),$$

$$\begin{aligned} f(\sigma_m) &= \frac{1}{2} (\varepsilon - 1 - (\varepsilon + 1)\sigma_m) \\ &= \begin{cases} \varepsilon & \text{if } \sigma_m = -1, \\ -1 & \text{if } \sigma_m = +1. \end{cases} \end{aligned} \quad [5]$$

The motivation for this expression for $f(\sigma_m)$ comes from ref. 22, where it is related to $h_m = \varepsilon M_{-m} - M_{+m}$, with M_{+m} and M_{-m} being, respectively, the numbers of ordered (+) and disordered (−) grains above grain m . The dynamics imposes (23) the minimization of H_n , which is a complex procedure involving the often conflicting contributions of the opposing local fields h_n and j_n ; these comprise all of the factors $f(\sigma_m)$ (which take values ε or -1 according to Eq. 5) coming from all of the other grains m in the column.

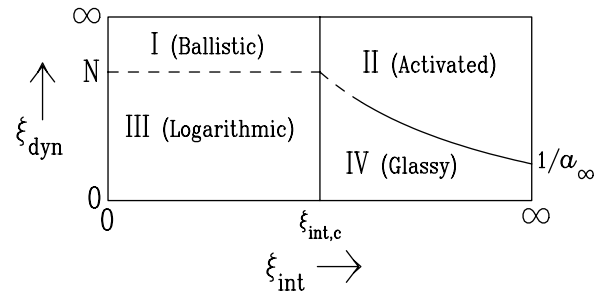


Fig. 3. Schematic zero-temperature dynamical phase diagram of the model of ref. 23 in the $\zeta_{\text{int}} - \zeta_{\text{dyn}}$ plane, showing the four dynamical phases revealed and investigated in the text.

Probing a Granular Column: Interrelationship of Theory and Simulations.

The ground states of this model, as well as their zero-temperature dynamics [the dynamics of how a ground state is spontaneously reached (26)] are extremely heterogeneous, and depend (23) strongly on the ratio of ζ_{int} and ζ_{dyn} , in terms of the system size N . They are most easily classified in terms of an ordering length $L(t)$, which represents the extent of propagation of order in the system at any given time. Each part of the phase diagram shown in Fig. 3 can be associated with a particular part of a real column—its top, bottom, or middle—in a way that will be described below.

Ballistic phase: ζ_{int} small with respect to N , ζ_{dyn} large and comparable with N . Here, grains feel hardly any frustration (small ζ_{int}) and are scarcely hindered by the weights of the grains above them (large ζ_{dyn}). This is appropriate to grains near the top (free surface) of a granular column; zero-temperature dynamics causes the ordering length $L(t)$ to propagate ballistically from top to bottom (see Fig. 4), hence the name ballistic (see Fig. 3). This is visible in a movie (see [Movie S1](#)) made on a sample run of our model in the ballistic phase (23). Each of its 320 frames corresponds to one configuration of a column of 100 grains. Red and yellow correspond respectively to disordered and ordered orientations of grains; note the propagation of an “ordering wave” down the column.

Logarithmic phase: ζ_{int} and ζ_{dyn} both small with respect to N . Grains here experience little frustration, but begin to feel the weights of grains above them; this phase corresponds to the region between the top and middle of a column. The ordering length $L(t)$ propagates logarithmically slowly (see Fig. 4), hence the name logarithmic (see Fig. 3). Both this and the ballistic phase were already present in the model of ref. 22, where depth-dependent density fluctuations were observed, in satisfying agreement with the independent simulation results of Fig. 1.

Activated phase: ζ_{int} and ζ_{dyn} both large and comparable with N . Here, frustration (large ζ_{int}) severely inhibits the search for the ground states, although relatively fast grain dynamics (large ζ_{dyn}) are observed. Ground states are reached purely by chance, usually after long times, as every new orientation of a grain potentially destabilizes grain orientations below and above itself. The motion of $L(t)$ whereby this occurs (see Fig. 4) corresponds to an activated process, hence the name of the corresponding phase (Fig. 3). Such dynamics prevail in the region between the middle and the base of the column (23).

Glassy phase: ζ_{int} large and comparable with N , ζ_{dyn} small with respect to N . Here, grain dynamics are both slow (small ζ_{dyn}) and heavily frustrated (large ζ_{int}). The time for the system to jam is very long, reflecting the fact that long-range interactions are really registered by slowly moving grains; intermittency (Fig. 4) is manifested in the way $L(t)$ approaches an attractor. There is a noticeable absence of a propagating wave from top to bottom; rather, the system hovers slowly between two nearly fully polar-

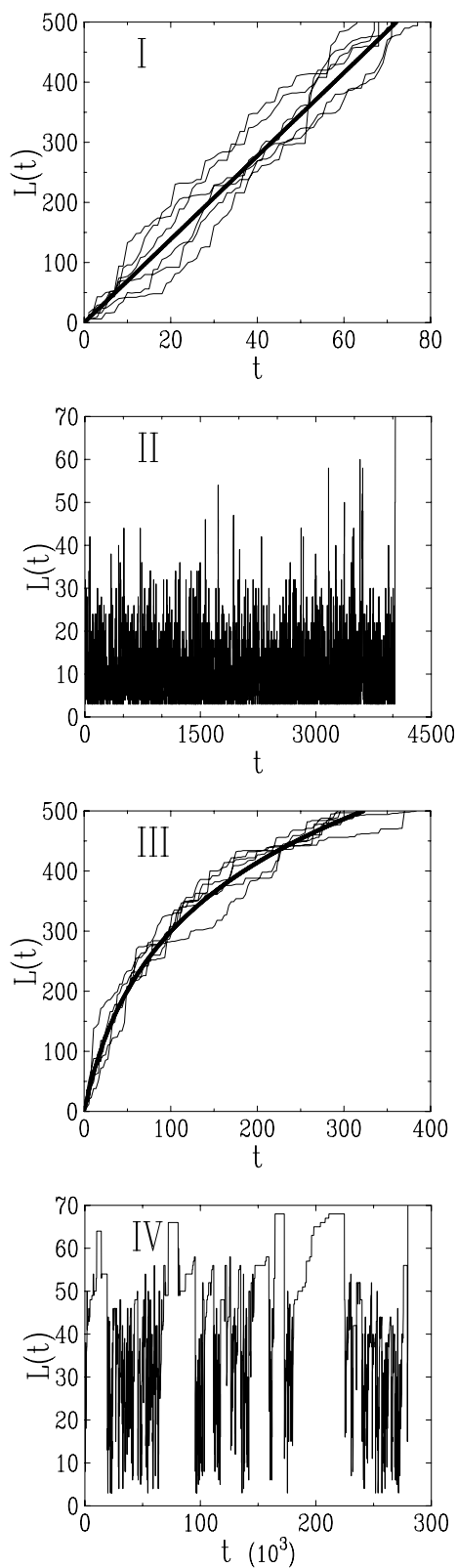


Fig. 4. Plots (23) of the thickness $L(t)$ of the upper ordered layer of the column against time t , illustrating the four dynamical phases. I: Ballistic phase (several tracks with $\zeta_{\text{int}} = 3$, $\zeta_{\text{dyn}} = \infty$, $N = 500$). II: Activated phase (one single track with $\zeta_{\text{int}} = 50$, $\zeta_{\text{dyn}} = \infty$, $N = 70$). III: Logarithmic phase (several tracks with $\zeta_{\text{int}} = 3$, $\zeta_{\text{dyn}} = 200$, $N = 500$). The thick line shows the analytic result obtained for logarithmic behavior in ref. 23. IV: Glassy phase (one single track with $\zeta_{\text{int}} = 50$, $\zeta_{\text{dyn}} = 7$, $N = 70$).

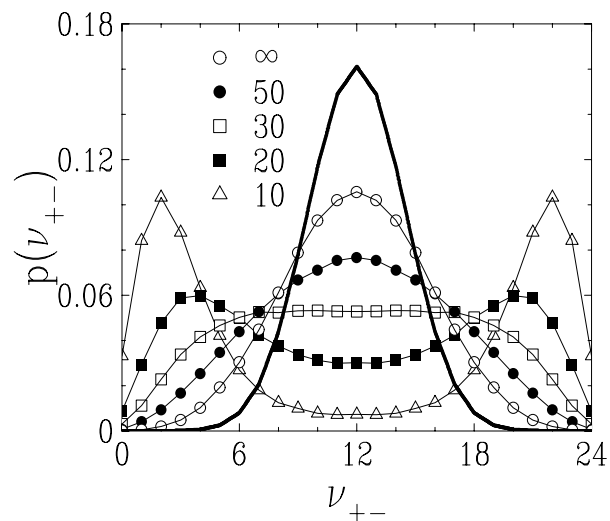
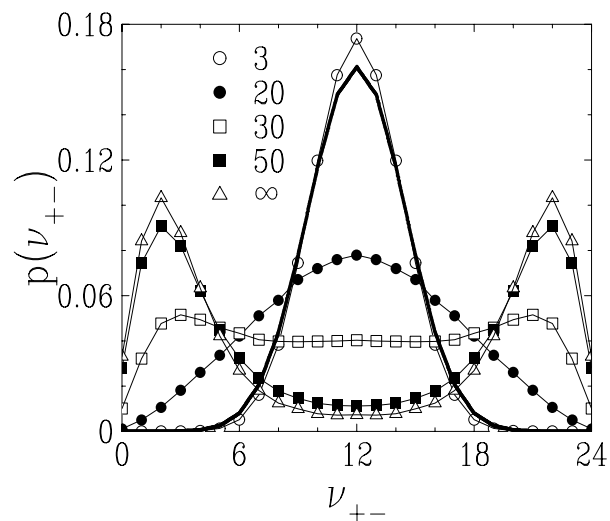
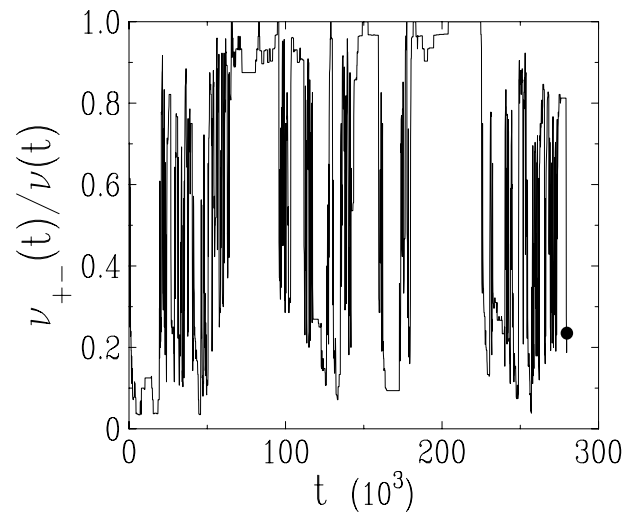


Fig. 5. Using dimer orientations to explore the phase diagram. (Top) A plot of the fraction $\nu_{+-}(t)/\nu(t)$ of $(+-)$ dimers, for the history illustrating Phase IV in Fig. 4. Full symbol: value of the observable in the attractor, i.e., right at the jamming time T . (Middle and Bottom) Histogram plots of the probability distribution $p(\nu_{+-})$ for $N = 50$ (hence $\nu = 24$), respectively for $\zeta_{\text{dyn}} = 10$ and variable $\zeta_{\text{int}} = \infty$ and variable ζ_{dyn} . The binomial distribution is shown as thick full lines (from ref. 23).

ized states until it jams. Such glassy (Fig. 3) dynamics are predicted (23) to exist near the very bottom of the column.

Cross-Over Phenomena; Homing into the Glassy Phase. Apart from describing each of the phases mentioned above, our model is also able to shed light on the cross-overs between the different phases. That between the ballistic and the activated phase has been described (23) by a model involving drift and diffusion; the propagation of the ordered layer $L(t)$ toward the base is visualized as the motion of an effective particle in a biased (gravitational) potential, whose velocity V at a given point in phase space is proportional to the difference between the space-averaged effects of the two local fields h (parallel to the gravitational field) and j (against the gravitational field). Thus, near the top of the column where h overwhelms j , the velocity V adds to the gravitational bias, and $L(t)$ propagates ballistically fast. As one approaches the middle of the column, j becomes progressively more effective until a purely diffusive point is reached where it perfectly cancels out the h field on average. Further down, as j begins to predominate over h , the drift velocity V of the effective particle changes sign, so that it becomes negative with respect to the gravitational bias; drift now opposes the downward propagation of $L(t)$ to reach the columnar base, and the ground state is found after many such oppositions by an activated process.

An additional cross-over that we have been able to describe via another effective model (23) is that between the activated and the glassy regimes, which involves increasingly slower “clocks” of frequency ω_n , as increasingly deep levels n of the column are probed. Our model suggests that the jamming time is always the larger of two times: the entropic time (the time taken to probe all of the layers corresponding to each clock) and that corresponding to the time scale of the slowest clock. In the middle region of a real column, where even the lowest layer has relatively fast dynamics, the jamming time is the entropic one; this corresponds to the activated regime. On the other hand, when the number of local clocks is essentially equal to the total number N (as occurs near the base of a long column), the jamming time corresponds to the largest time scale in the system, which is that of the deepest layer ($T_N = 1/\omega_N$). This simple reasoning actually gives good qualitative agreement with the full numerical solutions obtained in ref. 23.

The glassy phase is the richest phase of our model, and was investigated at greater length than the others. Although our model is able to describe ground states of arbitrary symmetry, we chose for simplicity a system whose ground states were dimerized, to carry out this detailed exploration. A major observation (23) is that whereas any of the $2^{N/2}$ dimerized ground states of an N -grain column are equally likely to be attained in the ballistic, logarithmic, and activated phases, the glassy phase is special in its choice of two “intrinsic” states—the “crystalline” (fully polarized) ground states (+-+-+- or -+-+-+). Under zero-temperature dynamics, trajectories in the glassy phase of our model approach them only in the asymptotic limit, and with a great deal of intermittency, as shown by the ordering length $L(t)$ (see bottom plot in Fig. 4). Other quantities of interest, such as the fraction of +- dimers, also manifest a similar intermittency in the glassy phase en route to jamming (see uppermost plot of Fig. 5); the details of these investigations are presented in ref. 23. The characteristic (26, 27) feature of such intermittency is that quiescent periods (when the system lingers in the vicinity of one of the two crystalline intrinsic states) are separated by periods of itinerancy, when configurations are randomly explored via strong systemic fluctuations. This is visible in a movie (see [Movie S2](#)) made on a sample run of our model in the glassy phase (23). Red and yellow correspond,

respectively, to disordered and ordered orientations of grains. Each of the 320 frames corresponds to one configuration of a column of 70 grains. The first 160 frames correspond to the beginning and the last 160 to the end configurations of a trajectory comprising 25,026 configurations, which are separated by 25 blank frames to mark the discontinuity. Notice the absence of an ordering wave here; the system hovers between different ground states and ends near one of the crystalline ones.

The cross-over to the glassy phase from the logarithmic and activated phases is continuously obtained by varying ζ_{int} and ζ_{dyn} , respectively; representative plots are presented in the two lower plots of Fig. 5, where the histograms of +- dimers are plotted for a range of parameter values. In the first of these, ζ_{dyn} is fixed at a low value, whereas ζ_{int} is progressively increased, depicting the cross-over to the glassy from the logarithmic phase; the bottom plot of Fig. 5 depicts the cross-over from activated to glassy, as ζ_{int} is fixed at a high value, and ζ_{dyn} decreases progressively. The trends in the two plots are virtually identical; the distribution of +- dimers is close to binomial in the activated/logarithmic phases, because the ground states include all possible combinations of dimers. With the parameter shift to the glassy phase in both plots, the histogram approaches a two-peaked distribution, with each peak centered on one of the two intrinsic states mentioned above.

The above clearly implies the existence of underlying ground states of crystallinity [intrinsic states (26)] in the glassy phase of our model, as distinct from the other three phases. It is important to emphasize that all of the dynamics considered in our model (23) are zero-temperature dynamics; clearly the application of finite-temperature dynamics would lead one to a sheaf of higher-energy, metastable states. This picture of an energy landscape where intrinsic crystalline states underlie a range of metastable states accessible at finite temperatures is characteristic of glassy systems (26, 27) and is a retrieval of earlier results found in the jammed phase of granular media modeled via random graphs (28).

Concluding Remarks

The experimental questions that motivated our investigations concerned the depth-dependence of density fluctuations and the mysterious presence of “metastable states” in the “lower portion of the column” of ref. 6; the simulation results presented here, in conjunction with the theoretical framework of ref. 23 address both these issues. We have shown by a combination of analytical and numerical techniques that strong heterogeneities are manifest as a function of depth in a granular column; they arise from a complex juxtaposition of effects due to frustration and gravity. Although it is true that the similarities of behavior predicted from theory and simulation remain qualitative so far, the independence of these two approaches reinforces the robustness of their common conclusions. In particular, we have provided a framework that explains the metastability observed in the lower portion of the experimental column of ref. 6—this is likely due to the presence of the activated and glassy phases that our theoretical model (23) predicts. Finally, our results suggest that the strongest density fluctuations exist near the middle of the column.

ACKNOWLEDGMENTS. A.M. gratefully acknowledges the hospitality of the Institut de Physique Théorique, Saclay, France, and the Radcliffe Institute of Advanced Study, Harvard University, Cambridge, MA, where much of this work was done. This work was supported in part by National Science Foundation Grant DMR-0520513 through the Northwestern University Materials Research Science and Engineering Center, Chicago, IL, where it was completed. G.C.B. was supported by BBSRC, UK.

1. Mehta A (2007) *Granular Physics* (Cambridge Univ Press, Cambridge).
2. de Gennes PG (1999) Granular matter: A tentative view. *Rev Mod Phys* 88:5374–5382.

3. Blumenfeld R, Edwards SF, Ball RC (2005) Granular matter and the marginal rigidity state. *J Phys Condens Matter* 17:52481–52487.

4. Wittmer JP, Claudin P, Cates ME, Bouchaud J-P (1996) An explanation for the central stress minimum in sandpiles. *Nature* 382:336–338.
5. Ciamarra MP, Coniglio A, Nicodemi M (2006) Thermodynamics and statistical mechanics of dense granular media. *Phys Rev Lett* 97:158001.
6. Nowak ER, Knight JM, Ben-Naim E, Jaeger HM, Nagel SR (1998) Density fluctuations in vibrated granular materials. *Phys Rev E* 57:1971–1982.
7. Edwards SF (1994) The role of entropy in the specification of a powder. In *Granular Matter: An Interdisciplinary Approach*, ed Mehta A (Springer, New York) pp 121–140.
8. Langer, J (2004) Dynamics of shear-transformation zones in amorphous plasticity: Formulation in terms of an effective disorder temperature. *Phys Rev E* 70:041502.
9. Majmudar TS, Behringer RP (2005) Contact force measurements and stress-induced anisotropy in granular materials. *Nature* 435:1079–1082.
10. Erikson JM, Mueggenburg NW, Jaeger HM, Nagel SR (2002) Force distributions in three-dimensional compressible granular packs. *Phys Rev E* 66:040301(R).
11. Mehta A, Barker GC, Luck J-M (2004) Cooperativity in sandpiles: Statistics of bridge geometries. *J Stat Mech* P10014.
12. Brown RL, Richards JC (1966) *Principles of Powder Mechanics* (Pergamon, New York).
13. Mehta A, Barker GC (1993) Vibrated powders: A microscopic approach. *Phys Rev Lett* 67:394–397.
14. Barker GC, Mehta A (1991) Transient phenomena, self-diffusion, and orientational effects in vibrated powders *Phys Rev E* 47:184–188.
15. Staff author (1991) Shaking up powder physics—a model of what happens to individual grains in a pile of powder subjected to vibration. *Science News* July 27, 1991.
16. Silbert LE, Ertas D, Grest GS, Halsey TC, Levine D (2002) Geometry of frictionless and frictional sphere packings. *Phys Rev E* 65:031304.
17. D'Anna G, Mayor P, Gremaud G, Barrat A, Loreto V (2003) Extreme events-driven glassy behaviour in granular media. *Europhys Lett* 61:60–66.
18. D'Anna G, Gremaud G (2001) The jamming route to the glass state in weakly perturbed granular media. *Nature* 413:407–409.
19. Papoular M (1999) Dense suspensions and supercooled liquids: Dynamic similarities. *Phys Rev E* 60:2408–2410.
20. Weeks E, Crocker DE, Levitt AC, Schofield A, Weitz DA (2002) Three-dimensional direct imaging of structural relaxation near the colloidal glass transition. *Science* 287:627–631.
21. Stadler PF, Luck J-M, Mehta A (2002) Shaking a box of sand. *Europhys Lett* 57:46–52.
22. Mehta A, Luck J-M (2003) Why shape matters in granular compaction. *J Phys A* 36:L365–L372.
23. Luck J-M, Mehta A (2007) Dynamical diversity and metastability in a hindered granular column near jamming. *Eur Phys J B* 57:429–451.
24. Liu AJ, Nagel SR (1998) Jamming is not just cool anymore. *Nature* 396:21–22.
25. Kob W, Donati C, Plimpton SJ, Poole PH, Glotzer SC (1997) Dynamical heterogeneities in a supercooled Lennard-Jones liquid. *Phys Rev Lett* 79:2827–2830.
26. Mézard M, Parisi G, Virasoro MA (1987) *Spin Glass Theory and Beyond* (World Scientific, Singapore).
27. Toninelli C, Biroli G, Fisher DS (2006) Jamming percolation and glass transitions in lattice models. *Phys Rev Lett* 96:035702.
28. Berg JM, Mehta A (2002) Glassy dynamics in granular compaction: Sand on random graphs. *Phys Rev E* 65:031305.